

# The Effect of Rotational Gravity Darkening on Magnetically Torqued Be Star Disks

J. C. Brown,<sup>1</sup> D. Telfer,<sup>1</sup> Q. Li,<sup>1,4</sup> R. H. Anuschkik,<sup>2</sup> J. P. Cassinelli,<sup>3</sup> and A. Kholtygin<sup>5,6</sup>

<sup>1</sup>Dept. of Physics and Astronomy, University of Glasgow, Glasgow, G12 8QQ, UK;

<sup>2</sup>European Southern Observatory, Karl-Schwarzschild-Str. 2, 85748 Garching, Germany;

<sup>3</sup>Dept. of Astronomy, University of Wisconsin-Madison, USA;

<sup>4</sup>Dept. of Astronomy, Beijing Normal University, China;

<sup>5</sup>Astronomical Institute, St. Petersburg University, Saint Petersburg State University,

V. V. Sobolev Astronomical Institute, 198504 Russia;

<sup>6</sup>Isaac Newton Institute of Chile, St. Petersburg Branch

Accepted . Received ; in original form

## ABSTRACT

In the magnetically torqued disk (MTD) model for hot star disks, as proposed and formulated by Cassinelli et al. (2002), stellar wind mass loss was taken to be uniform over the stellar surface. Here account is taken of the fact that as stellar spin rate  $S_0$  ( $= \frac{v_p}{\sqrt{R^3/GM}}$ ) is increased, and the stellar equator is gravity darkened, the equatorial mass flux and terminal speed are reduced, compared to the poles, for a given total  $\dot{M}$ . As a result, the distribution of equatorial disk density, determined by the impact of north and southbound flows, is shifted further out from the star. This results, for high  $S_0$  ( $> 0.5$ ), in a fall in the disk mass and emission measure, and hence in the observed emission line EW, scattering polarization, and IR emission. Consequently, contrary to expectations, critical rotation  $S_0 \approx 1$  is not the optimum for creation of hot star disks which, in terms of EM for example, is found to occur in a broad peak around  $S_0 \approx 0.5 - 0.6$  depending slightly on the wind velocity law.

The relationship of this analytic quasi-steady parametric MTD model to other work on magnetically guided winds is discussed. In particular the failures of the MTD model for Be-star disks alleged by Owocki & ud-Doula (2003) are shown to revolve largely around open observational tests, rather in the basic MTD physics, and around their use of insufficiently strong fields.

Subject headings: stars: emission-line, Be { stars: magnetic fields { stars: mass loss { stars: rotation { stars: winds, outflows { polarization.

---

<sup>1</sup>Send off print requests to: john@astro.gla.ac.uk (JCB); li@astro.gla.ac.uk (QL)

## 1. Introduction

Be stars are defined as 'non-supergiant B-type stars whose spectra have, or had at one time, one or more Balmer lines in emission' (Collins 1987). The pioneering research on Be stars by Struve proposed a rotational model with emission lines from equatorial disks (Struve 1931), but Be star disks remain enigmatic despite many decades of detailed observations and research (Jaschek & Groth 1982; Slettebak 1982; Underhill & Doazan 1982; Slettebak & Snow 1987; Slettebak 1988; Smith et al. 2000; Porter & Rivinius 2003). The main physics problems they pose are how the material in them (a) is delivered from the star; (b) becomes so dense; (c) acquires such high angular momentum. The answer to (a) undoubtedly lies in stellar radiation pressure. The first qualitative answer to (b) was the Wind Compressed Disk (WCD) model of Bjorkman & Cassinelli (1993). In this, the angular momentum of rotating wind flow returns the matter to the equator where north and south streams collide and create a shock compressed disk. There are several snags with this model. Firstly, it does not produce high enough densities. Secondly, the disk formed has mainly radial flows rather than the quasi-Keplerian azimuthal flows observed. Thirdly, non-radial line-driving forces (Owocki et al. 1996) may cause polar rather than equatorial flow to dominate.

A phenomenological solution to these problems was proposed and quantified parametrically in the Magnetically Torqued Disk (MTD) model of Cassinelli et al. (2002). This invokes a dipole-like field which steers the wind flow toward the equator and torques up its angular momentum on the way. The field torques up the wind flow to Keplerian speeds or higher and connects the radial flow redirecting it to be poloidal and creating a shock compressed equatorial disk. The isothermal disk grows in thickness (but not in density) over comparatively long timescales (years) which are roughly consistent with long time-scale variability of some Be stars (Doazan 1982; Dachs 1987; Okazaki 1997; Telting 2000), allowing a quasi-steady treatment. There is growing observational evidence of reasonably strong fields (hundreds of Gauss) in hot stars | e.g.,  $\delta$  Orionis with  $B_{\text{pole}} = 530 - 230$  G (Neiner et al. 2003),  $\epsilon$  Cephei with  $B_{\text{pole}} = 360 - 30$  G (Donati et al. 2001),  $\gamma$  Orionis C with  $B_{\text{pole}} = 1100 - 100$  G (Donati et al. 2002), though some of these are very oblique and/or slow rotating and the MTD model not directly applicable in its basic form.

In the MTD treatment the stellar wind mass flux and wind speed were taken to be uniform over the stellar surface. For the case of a rotating star, essential to creating a disk, this assumption is invalid. Rotation results in equatorial gravity darkening which reduces the wind mass flux and speed there, as described by Owocki et al. (1998). In this paper, we evaluate the effects of this on the MTD model. We do so by generalising the basic quasi-steady parametric approach of MTD, but discussing in Section 5 issues concerning the properties of that description in relation to other theoretical and observational work on

the problem. The MTD paper was really the first to model the combined effects of field and rotation but several earlier papers had discussed disk formation by magnetic channeling (Matt et al. 2000), while work subsequent to MTD has variously challenged it (Owocki & ud-Doula 2003), and supported it (Maheswaran 2003). Insofar as there remains a degree of disagreement in the literature over whether the model works for Be stars, our detailed results should be treated with some caution, though the general trends of the effect of gravity darkening should be sound.

## 2. Effect of Gravity Darkening on Disk Density

Owocki et al. (1998) showed that the mass flux from a stellar surface satisfies

$$F_{m_o}(\theta) \propto g; \quad (1)$$

while the terminal speed satisfies

$$v_1(\theta) \propto g^{1/2}; \quad (2)$$

where  $g$  is the local effective gravity.

On a rotating sphere with stellar radius  $R$  and angular velocity  $\omega$ , at colatitude  $\theta$ , the net gravity is

$$\begin{aligned} g(\theta) &= \frac{GM}{R^2} - \frac{(\omega R \sin \theta)^2}{R \sin \theta} \\ &= \frac{GM}{R^2} - \omega^2 R \sin^2 \theta \\ &= g_o \left( 1 - \frac{(\omega R)^2}{GM/R} \sin^2 \theta \right) \\ &= g_o \left( 1 - S_o^2 \sin^2 \theta \right); \end{aligned} \quad (3)$$

where  $S_o = \omega \sqrt{\frac{R^3}{GM}}$  as in MTD. Strictly speaking, we should also include the effect of continuum scattering radiation pressure at least, which results in  $g_o = \frac{GM}{R^2} (1 - \tau_{rad})$ , where  $\tau_{rad} = \frac{L}{L_{Edd}}$  is the ratio of the stellar luminosity to the Eddington luminosity (Meador & Meynet 2000).

It follows that the mass flux at  $\theta$  becomes

$$F_{m_o}(\theta) = K \left( 1 - S_o^2 \sin^2 \theta \right); \quad (4)$$

where  $K$  is a constant, and the terminal speed for matter from  $\theta$  is

$$v_1(\theta) = v_{1_o} \left( 1 - S_o^2 \sin^2 \theta \right)^{1/2}; \quad (5)$$

{ 4 {

where  $v_{10}$  is the value of  $v_1$  at  $\theta = 0$ .

Here we will assume the wind velocity obeys  $v_w(r) = v_1 (1 - \frac{R}{r})$ , but with

$$v_w(r; \theta) = v_1(\theta) \left(1 - \frac{R}{r}\right); \quad (6)$$

where  $\theta$  is assumed not to depend on  $r$ . This basically requires that wind acceleration occurs quite near the star and that the field lines are roughly radial there. We want to express  $K$  in terms of the total mass loss rate  $\dot{M}$

$$\begin{aligned} \dot{M} &= \int_{\theta=0}^{\theta_0} F_{m0}(\theta) 2R \sin \theta d\theta \\ &= 4R^2 K \int_0^{\theta_0} (1 - S_0^2 \sin^2 \theta) \sin \theta d\theta \\ &= 4R^2 K \left(1 - \frac{2S_0^2}{3}\right); \end{aligned} \quad (7)$$

So by equation (4),

$$F_{m0}(\theta) = \frac{\dot{M}}{4R^2 \left(1 - \frac{2S_0^2}{3}\right)} (1 - S_0^2 \sin^2 \theta); \quad (8)$$

To relate this mass flux at  $\theta$  on the stellar surface to that normal to the equatorial plane at distance  $x = r=R$ , we follow Cassinelli et al. (2002) in parametrizing the decline of magnetic field,  $B$ , with equatorial plane distance according to

$$B(x) = B_0 x^{-b}; \quad (9)$$

where  $B_0$  is taken as uniform over, and normal to, the stellar surface, and  $b$  is a constant with a dipole field  $b = 3$ . Flux conservation then requires that a cross-sectional area  $dA$  of a flux tube arriving at the equator is related to its area  $dA_0$  at the star by  $B dA = B_0 dA_0$  or

$$dA(x) = dA_0 x^b; \quad (10)$$

However,  $dA(x) = 2R^2 x dx$  and  $dA_0 = 2R^2 \sin \theta d\theta$  so that the relation between  $\theta$  and  $x$  is given by integrating  $\sin \theta d\theta = x^{b+1} dx$ , to yield

$$\cos \theta = C \frac{x^{b+2}}{b+2}; \quad (11)$$

Requiring that  $x \rightarrow 1$  for  $\theta \rightarrow 0$  implies  $C = 1$  so that

$$\cos \theta(x) = 1 - \frac{x^{b+2}}{b+2}; \quad (12)$$

For the particular case  $b = 3$  (the dipole case) mainly discussed by Cassinelli et al. (2002), and which we focus on henceforth, this yields

$$\cos(\alpha) = 1 - \frac{1}{x} \quad (13)$$

We can now obtain the mass flux  $F_m(x)$  at  $x$  near the equatorial plane by using  $F_m(x) = \int_{\text{disk}} \rho v \, dA$  and using equations (8), (10) and (13), namely

$$F_m(x) = \frac{M - v_1^2}{4 R^2 (1 - 2S_o^2)} x^3 f_1 S_o^2 \left[ 1 - \left(1 - \frac{1}{x}\right)^2 \right] g; \quad (14)$$

while by equations (5), (6) and (13), the wind speed there is

$$v_w(x) = v_1 \left(1 - \frac{1}{x}\right) f_1 S_o^2 \left[ 1 - \left(1 - \frac{1}{x}\right)^2 \right] g^{1/2}; \quad (15)$$

and the arriving wind ram pressure  $P_{\text{ram}}(x) = F_m(x) v_w$  is

$$P_{\text{ram}} = \frac{M - v_1^2}{4 R^2} x^3 \left(1 - \frac{1}{x}\right) \frac{f_1 S_o^2 \left[ 1 - \left(1 - \frac{1}{x}\right)^2 \right] g^{3/2}}{1 - 2S_o^2}; \quad (16)$$

The high density  $\rho_D(x)$  of cool, shock-compressed, disk (WCD) in the equatorial plane is then given as in the WCD model (and in MTD) by the isothermal disk (sound speed  $c_s$ ) pressure balance expression  $\rho_D c_s^2 = P_{\text{ram}} = P_D$  or by equation (16)

$$\rho_D(S_o; x) = \rho_o x^3 \left(1 - \frac{1}{x}\right) \frac{f_1 S_o^2 \left[ 1 - \left(1 - \frac{1}{x}\right)^2 \right] g^{3/2}}{1 - 2S_o^2}; \quad (17)$$

Here

$$\rho_o = \frac{M - v_1^2}{4 R^2 v_1} \left(\frac{v_1}{c_s}\right)^2 \quad (18)$$

which is equivalent to  $\rho_{Dc}$  in the MTD model. Based on equation (17), we can write the disk density allowing for rotational gravity darkening, compared to that neglecting it (e.g., MTD) as

$$\left(\frac{\rho_D(S_o; x)}{\rho_D(0; x)}\right) = \frac{\left[ 1 - \frac{S_o^2}{x} \left(2 - \frac{1}{x}\right) \right]^{3/2}}{1 - 2S_o^2} \quad (19)$$

with the property  $\left(\frac{\rho_D(S_o; 1)}{\rho_D(0; 1)}\right) = \left(1 - 2S_o^2\right)^{3/2} = \left(1 - 2S_o^2\right)^{3/2}$  which is  $< 1$  for all  $S_o$ , and tends to 0 as  $S_o \rightarrow 1$ . This is because the equatorial wind flow falls with increasing  $S_o$ , reducing the inner disk compression. On the other hand, if we (formally) see comments below in Section 3) apply equation (19) as  $x \rightarrow 1$  we would get for the disk behavior

$$\left(\frac{\rho_D(S_o; 1)}{\rho_D(0; 1)}\right) \rightarrow \frac{1}{1 - 2S_o^2}; \quad (20)$$

This is always  $> 1$  because the polar wind supply of mass to large, equatorial distances  $x$ , is increased (for fixed  $M$ ) for large  $S_o$ . Also, as  $S_o \rightarrow 1$  (critical rotation) we find

$$(1; x) = 3 \left(1 - \frac{1}{x}\right)^3 \tag{21}$$

which is  $> 1$  at  $x > 3^{1/3} = (3^{1/3} - 1) \approx 3.26$ . In Figs. 1 and 2, we show  $\frac{d}{d}$  and  $(S_o; x)$  versus  $x$  for various  $S_o$ . Fig. 1 shows the disk density to peak in the range  $x \approx 1.3 - 2.3$  for all  $S_o$ , then to decrease rapidly with  $x$  for all  $S_o$ .

### 3. Effect of Gravity Darkening on Disk Extent, Mass, and Emission Measure

We have seen that  $\rho_D(x)$  decreases and moves its maximum somewhat to larger  $x$  values as  $S_o$  increases. However, we need also to consider the extent of the disk, i.e., the lower and upper boundaries of equation (17) in  $x$  as limited by the magnetic field strength. While enhancement of  $\rho_D$  locally enhances the local contribution per unit volume ( $\frac{d}{d}$ ) to the disk emission measure, it makes the material there harder to torque so that the extent of the disk is modified. In particular, for example, equation (20) is not valid in practice since the rapid decline in  $B(x)$ , as  $x$  goes up, limits the torquing to a finite distance.

To estimate the effect of including rotational gravity darkening on observable disk properties, we need to assess the effect on the inner and outer disk boundaries. Here we do so using a somewhat simpler treatment than that in MTD, namely what MTD termed the 'switch approximation'. In this, the disk is taken to be rigidly torqued by the magnetic field (i.e.,  $v = v_o x$ , where  $v_o = S_o \sqrt{GM/R}$ ) out to the distance where the magnetic energy density  $\frac{B^2}{8}$  falls below the rotational kinetic energy density  $U_{KE} = \frac{1}{2} \rho_D v^2$ . We have then, by equation (9),

$$U_B = \frac{B^2}{8} = \frac{B_o^2}{8} x^{-6} \tag{22}$$

and by equation (17)

$$U_{KE} = \frac{1}{2} \rho_o \frac{GM}{R} S_o^2 x^{-1} \left(1 - \frac{1}{x}\right) \frac{f1 S_o^2 [1 - (1 - \frac{1}{x})^2] g^{3=2}}{1 - 2S_o^2=3} : \tag{23}$$

So the outer disk boundary  $x = x_{outer}(S_o; )$  is given by setting  $U_B = U_{KE}$ . Thus  $x_{outer}$  is the solution  $x$  to

$$x^5 \left(1 - \frac{1}{x}\right) \frac{f1 S_o^2 [1 - (1 - \frac{1}{x})^2] g^{3=2}}{1 - 2S_o^2=3} = \frac{2}{S_o^2}; \tag{24}$$

where

$$= \left(\frac{B_o^2=8}{GM_o=2R}\right)^{1=2} \tag{25}$$

is a measure of field energy compared to the disk gravitational energy. The inner disk boundary in the present approximation is simply the Keplerian rotation distance (c.f., MTD)

$$x_{\text{inner}} = S_o^{2=3}; \tag{26}$$

#### 4. Results and Discussion

In Figs. 3 and 4, we show  $x_{\text{inner}}(S_o)$  and  $x_{\text{outer}}(S_o)$  versus  $S_o$  for various  $\beta$  values, and the corresponding colatitudes, on the stellar surface, of  $x_{\text{inner}}$  and  $x_{\text{outer}}$  in terms of equation (13). It turns out that these boundaries do not change greatly with  $S_o$  once  $S_o$  is larger than 0.2 | 0.3, but change a lot with  $\beta$ , and that the mass flux reaching the disk comes from a rather small range of colatitudes (e.g. for  $S_o = 0.6, 45^\circ \dots 70^\circ$  with  $\beta = 6$  | see Fig. 4). Mass flow from the pole (small  $\beta$ ) leaves the star as part of the wind while equatorial flow (large  $\beta$ ) does not achieve Keplerian speed.

According to equation (25),  $\beta$  is determined by the magnetic and gravitational fields. In order to make mass flux channeling and torquing possible,  $\beta$  has to be substantially greater than unity. In terms of observations, the magnetic fields of Be stars are no larger than hundreds of Gauss. Hence,  $\beta$  should probably be in the range of  $1 \text{ ! } 10$  for Be stars to meet this requirement. In Figs. 3 and 4, we also see that for smaller  $\beta$ , a larger  $S_o$  is necessary for a disk (clearly, the outer radius of the disk must be larger than the inner radius). These two figures also show that the gravity darkening has a small effect on the outer radius of the disk, which is within  $5R$  for appropriate  $\beta$  and  $S_o$ . Similar outer boundaries have been derived for some stars using different disk models by Dougherty et al. (1994) and Cote et al. (1996).

The detection of disks by polarization, infrared emission, and emission line strength is related to their mass and their emission measure which are proportional to  $\int_V \rho_D dV$  and  $\int_V \rho_D^2 dV$ , respectively, where  $V$  is the disk volume. If the disk has thickness  $H(x) = h(x)R$  at distance  $x$  then it contains a total number of particles

$$N = \frac{2 R^3}{m} \int_{x_{\text{inner}}(S_o)}^{x_{\text{outer}}(S_o)} \rho_D(x) h(x) x dx; \tag{27}$$

and has emission measure

$$EM = \frac{2 R^3}{m^2} \int_{x_{\text{inner}}(S_o)}^{x_{\text{outer}}(S_o)} \rho_D^2(x) h(x) x dx; \tag{28}$$

where  $m$  is the mean mass per particle. Using equation (17) these yield

$$N = N_o \int_{x_{\text{inner}}(S_o)}^{x_{\text{outer}}(S_o)} \frac{x^2 h(x)}{1 - 2S_o^2=3} \left(1 - \frac{1}{x}\right) f_1 S_o^2 \left[1 - \left(1 - \frac{1}{x}\right)^2\right]^{3=2} dx; \tag{29}$$

where  $N_o = 2 R \frac{3 \sigma}{m}$ , and

$$EM = EM_o \int_{x_{inner}(S_o)}^{x_{outer}(S_o)} \frac{x^5 h(x)}{(1 - 2S_o^2)^2} \left(1 - \frac{1}{x}\right)^2 \frac{1}{x} \left[1 - \left(\frac{1}{x}\right)^2\right]^3 dx; \quad (30)$$

where  $EM_o = 2 R^3 \left(\frac{\sigma}{m}\right)^2$ .

Following the Brown & McLean (1977) formulation, the scattering polarization is  $P = (1 - 3) \sin^2 i$ , where  $\mu$  is optical depth,  $\mu_p$  is the shape factor of the disk and  $i$  is the inclination angle. Assuming the disk to be a slab with constant thickness  $H = Rh$  and including the finite source depolarization factor  $D = \frac{1}{\sqrt{1 - R^2/r^2}} = \frac{1}{\sqrt{1 - 1/x^2}}$  (Cassinelli et al. 1987; Brown et al. 1989), then we have the optical depth

$$\begin{aligned} &= \frac{3 \tau}{16} \int_{r_1}^{r_2} \int_{z_1}^{z_2} n(r; z) D(r) dr dz \\ &= \frac{3 \tau R}{16} \int_{x_{inner}}^{x_{outer}} \int_0^h n(x; z) D(x) \frac{x}{x^2 + z^2} dx dz \\ &= \int_{x_{inner}}^{x_{outer}} x^3 \left(1 - \frac{1}{x}\right)^2 \frac{\left[1 - S_o^2 \left(\frac{2}{x} - \frac{1}{x^2}\right)\right]^3}{1 - 2S_o^2} \frac{1}{x^2} \arctan \frac{h}{x} dx; \end{aligned} \quad (31)$$

where  $\sigma_o = \frac{3 \tau R \sigma}{16 m}$ ,  $\tau$  is Thomson cross section,  $n = N_D = m$  is the electron density of the disk, and  $\mu$  is the cosine of the angles between the incident light to the disk and the rotational axis. As in MTD, we neglect the absorption and suppose a fully ionized disk. The shape factor yields

$$\begin{aligned} &= \frac{R_{r_2} R_{z_2} \int_{r_1}^{r_2} \int_{z_1}^{z_2} n(r; z) D(r) dz dr}{R_{r_2} R_{z_2} \int_{r_1}^{r_2} \int_{z_1}^{z_2} n(r; z) D(r) dz dr} \\ &= \frac{\int_{x_{inner}}^{x_{outer}} n(x) D(x) \left[\frac{1}{2x} \arctan \frac{h}{x} - \frac{h}{2(h^2 + x^2)}\right] dx}{\int_{x_{inner}}^{x_{outer}} n(x) D(x) \arctan \frac{h}{x} dx}; \end{aligned} \quad (32)$$

Substituting equations (31) and (32) in the original polarization expression and after some reduction, yields the polarization,  $P$ , with gravity darkening effects,

$$P = P_o I_p \quad (33)$$

where  $P_o = \sigma_o = \frac{3 \tau R \sigma}{16 m}$  and  $I_p$  is the integral

$$I_p = \int_{x_{inner}}^{x_{outer}} x^3 \left(1 - \frac{1}{x}\right)^2 \frac{\left[1 - S_o^2 \left(\frac{2}{x} - \frac{1}{x^2}\right)\right]^3}{1 - 2S_o^2} \frac{1}{x^2} \arctan \frac{h}{x} dx (1 - 3) \sin^2 i; \quad (34)$$

Then  $I_p = P/P_o$  is found numerically and shown in Figs. 7 and 11 for  $h = 0.5$  with respect to typical half opening angles of the disk about  $10^\circ$ , (e.g., Hanuschik (1996); Porter (1996)), and the inclination angle  $i = 90^\circ$ .

In Figs. 5 and 6, we show the results of equations (29) and (30) for  $N(S_0; \beta)$  and  $EM(S_0; \beta)$  together with those obtained when gravity darkening is ignored (using same switch approximation). For the latter, we use the integrands as in equations (29) and (30), but with  $S_0 = 0$ ; the same lower limit  $x_{inner} = S_0^{2=3}$  as given by equation (26); and the outer limit the solution to equation (24), with  $S_0 = 0$  on the left. We see that increasing  $S_0$  from zero results in a rising disk mass and emission measure up to a broad maximum at  $S_0 \approx 0.5$  and falling back almost to 0 as  $S_0 \rightarrow 1$ . It is not surprising to see that gravity darkening has strong effects on total number of particles and emission measure, since gravity darkening effects significantly reduce the mass flow from equatorial stellar regions into the disk. We also note that  $N/N_0$  and  $EM/EM_0$  ratios have peaks at about  $S_0 \approx 0.5$  for all  $\beta$ , while for no gravity darkening they essentially keep increasing. Similar results are shown in Fig. 7 for the polarization which depends mainly on the disk electron scattering mass. The more the total number of particles in the disk, the stronger the polarization. If gravity darkening were neglected, one would get a large  $I_p$  so a small  $P_0$ , for a given observed polarization value  $P$  (equation 33). This would imply a smaller  $\beta$  since  $P_0 \propto \beta$ , which implies an underestimation of the mass loss rate  $\dot{M}$  (equation 18), if we ignore gravity darkening.

The previous treatment is for  $\beta = 1$ . In order to see the influence of the velocity law on the results, we tried various  $\beta$  values for a given  $\beta$ . Fig. 8 shows that wind velocity law has minor effects on the disk boundaries and so does gravity darkening. Figs. 9, 10 and 11 show that slower winds (i.e., bigger  $\beta$  values) will lead to much smaller total number of particles, emission measure and polarization of the disk, as well as gravity darkening significantly decreases these disk properties. From the plots we see that, for small  $\beta = 0.5$ , the total number of particles, emission measure and polarization peaks shift slightly to larger rotation rate ( $S_0 \approx 0.6$ ), while a statistical study of observation data indicates the most common  $S_0 \approx 0.7$  (Porter 1996) which, in our interpretation, would favor small  $\beta$ , i.e., fairly fast acceleration of winds from the stellar surface. If individual disk detectability peaks for  $S_0 \approx 0.6$  and actual detection peak for  $S_0 \approx 0.7$ , either there is a bias/selection effect in operation (Townsend et al. 2003), or there is an upward trend in the frequency distribution of  $S_0$  values.

## 5. Comparison of MTD with MHD Simulations and Other Work on Magnetic Channeling

It was noted in Section 1 that the MTD model is phenomenological and parametric, and not a full solution to the physics equations. It is aimed, like all such models, at describing the main features of a system accurately enough to reproduce the essential physics but simple

enough to facilitate ready incorporation of additional effects (such as gravity darkening) and comparisons with data. It is of course important to evaluate how well the MTD model describes the reality when compared with more complete solutions. A full and detailed comparison is beyond the scope of this paper but we summarise here the present status as we see it of the relation of MTD to recent analytic and numerical work on closely related problems.

One of the earliest studies of the problem which found disk formation was that in a 'magnetospheric' context was by Havnes & Goertz (1984). Keppens & Goedbloed (1999, 2000) carried out numerical simulations of magnetised stellar winds with rather weak fields and found disk 'stagnation zones' in the equatorial plane. Matt et al. (2000) studied non-rotating winds in dipole fields and found persistent equatorial disk structures around AGB stars though with a steady throughput of mass leaking through the disk. Maheswaran (2003) conducted a detailed analytic study of the MTD situation and found that persistent disks are formed for quite small fields though he obtained somewhat tighter constraints than MTD on the relevant regimes of magnetic field and spin rate. In the MHD simulations of isothermal flow driven outward from a non-rotating star with dipole magnetic fields, ud-Doula & Owocki (2002) found that the effect of magnetic fields in channeling stellar winds depends on the overall ratio of magnetic to flow kinetic energy density, (as did MTD) and obtained disk results with rather low fields.

In contrast to all of these, in the ud-Doula & Owocki (2003) conference paper, based on the same code as ud-Doula & Owocki (2002), the interpretation shifts somewhat and seems more negative about disk persistence. Owocki & ud-Doula (2003) added rotation to their earlier work and concluded that no stable disk could form, with matter either falling back or bursting out after a modest number of flow times. In fact, the MHD code they used is incapable of handling the larger fields which MTD argued were required and which are recently in fact observed (several hundred Gauss) in some Be stars, so their numerical results are not that relevant. Furthermore, given that observed fields are strong enough so that the wind is bound to be steered and torqued to the equatorial regions, if the behaviour of that matter were highly unstable as Ud-Doula and Owocki's simulation results, we should observe very frequent Be star disk disruption, which we do not. In fact we see no reason why material should fallback, given that it is centrifugally supported, until the dipole structure falls up. This takes a very large number of flow times (many years) - hence the the quasi-steady formulation in MTD. In the case of weak fields and low rotation, fallback and burst out of matter is not altogether surprising, but it is not clear why the Owocki & ud-Doula (2003) simulation results conflict with those of others. For stronger fields using order of magnitude scaling estimates, they found that disks, essentially like MTD can form and have gone on to develop scenarios for strong fields closely akin to MTD under the names Magnetically Rigid

Disk and Magnetically Confined Wind Shocked Disk. They were, however, dismissive of the relevance of this to Be-stars. This was not on the grounds of the physics of MTD but over the issue of whether a semi-rigid disk near co-rotation can be reconciled with observations of Be-stars, specifically spectrum line shapes and the long term V/R variations. The work of Telfer et al. (2003) suggests that the former is not a serious problem. The issue of the V/R variations was emphasised in the original MTD paper which recognised that, if MTD is the correct description of Be disk formation, a close examination is required of how the V/R variations could arise. At first sight it would seem that the conventional interpretation in terms of spiral density waves (induced by the non-spherical potential) in a Keplerian disk would not work if the field controlled the disk and another interpretation would have to be found but it depends on the rate of viscous diffusive redistribution of disk matter toward Keplerian (Maheswaran 2003). Until further testing is carried out we are therefore of the view that the MTD model remains a good basic scheme for further modelling work. We also note that, when MTD is applied across the range of hot star spectral types, it offers a remarkably good explanation of the narrow spectral range where disks are in fact detected. No other model offers any explanation of this observation.

## 6. Conclusions

We have discussed the phenomenological magnetically torqued disk (MTD) model of Cassinelli et al. (2002) for hot (particularly Be) star disk formation in relation to other work on magnetically steered wind creation of disk like structures, concluding that, for moderate fields comparable to those observed, the description is physically realistic but that further work is needed to see if its disk velocity structure can be reconciled with observations including line profiles and V/R variations. We have recognised that the basic model did not recognise the effect of spin induced gravity darkening on the latitudinal distribution of wind flow and consequently on disk density structure. We have included this effect and found that, although increasing  $S_0$  from zero favors disk formation, at high  $S_0$  the polar shift in mass flux results in decreasing disk detectability by emission or polarization. The fact that detectability (say above half of the height of the peak values of emission and polarization in Figs. 6, 7, 10, and 11) covers quite broad rotation range in  $S_0$ , namely  $S_0 = 0.25 - 0.80$ , is generally in good agreement with the fact that Be star rotation rates are typically estimated to occur most frequently near 0.7 (e.g., Porter (1996), and references therein; Yudin (2001)), which tends to favour fast acceleration velocity laws. Overall this means that in the MTD model, the most easily observable disks are, contrary to naive expectation, not expected from the fastest rotators, but from moderate ones, as observed, though we note the Townsend et al. (2003) comments on the effect of gravity darkening in

inferring underestimated line width rotation rates. Clearly the whole MTD scenario needs further work to test it thoroughly, including reconciliation of the phenomenology, numerical MHD, and analytic MHD theoretical treatments and work on further diagnostics such as X-ray emission from the MTD deceleration shocks of Be stars for comparison with ROSAT and other X-ray datasets.

#### Acknowledgements

The authors acknowledge support for this work from : U.K. PPARC Research Grant (JCB); NASA grant TM 3-4001A (JPC, JCB); and Royal Society Sino-British Fellowship Trust Award (QL), NSFC grant 10273002 (QL); RFBR grant 01-02-16858 (AK). An anonymous referee's comments lead to a significant improvement of the paper.

#### REFERENCES

- Bjorkman, J. E., & Cassinelli, J. P., 1993, *ApJ*, 409, 429
- Brown, J. C., Carlaw, V. A., & Cassinelli, J. P., 1989, *ApJ*, 344, 341
- Brown, J. C., & McLean, I. S., 1977, *A & A*, 57, 141
- Cassinelli, J. P., Brown, J. C., Maheswaran, M., Miller, N. A., & Telfer, D. C., 2002, *ApJ*, 578, 951
- Cassinelli, J. P., Nordsieck, K., & Murison, M. A., 1987, *ApJ*, 317, 290
- Collins, G. W., 1987, in *IAU Colloq. 92, Physics of Be Stars*, eds. A. Slettebak and T. P. Snow (Cambridge: Cambridge Univ. Press), 3
- Cote, J., Waters, L. B. F. M., & Marlborough, J. M., 1996, *A & A*, 307, 184
- Dachs, J., 1987, in *IAU Colloq. 92, Physics of Be Stars*, eds. A. Slettebak and T. P. Snow (Cambridge: Cambridge Univ. Press), 149
- Donati, J. F., Wade, G. A., Babel, J., Henrichs, H. F., de Jong, J. A., Harries, T. J., 2001, *MNRAS*, 326, 1265
- Donati, J. F., Babel, J., Harries, T. J., Howarth, I. D., Petit, P., Semel, M., 2002, *MNRAS*, 333, 55

- Doazan, V., 1982, in *B Stars with and without Emission Lines*, eds. A. Underhill & V. Doazan (NASA SP-456, Washington: NASA), 277
- Dougherty, S.M., Waters, L.B.F.M., Burki, G., Cote, J., Cramer, N., van Kerkwijk, M.H., & Taylor, A.R., 1994, *A & A*, 290, 609
- Jaschek, M., & Groth, H.G., eds. 1982, *IAU Symp. 98, Be Stars* (Dordrecht:Reidel)
- Hanuschik, R.W., 1996, *A & A*, 308, 170
- Havnes, O., & Goertz, C.K., 1984, *A & A*, 138, 421
- Keppens, R., Goedblbed, J.P., 1999, *A & A*, 343, 251
- Keppens, R., Goedblbed, J.P., 2000, *ApJ*, 530, 1036
- Maheswaran, M., 2003, *ApJ*, 592, 1156
- Maeder, A., & Meynet, G., 2000, *A & A*, 361, 159
- Matt, S., Balick, B., Winglee, R., & Goodson, A., 2000, *ApJ*, 545, 965
- Neiner, C., Hubert A.M., Fremat Y., Floquet M., Jankov S., Preuss O., Henrichs H.F., Zorec J., 2003, *A & A*, 409, 275
- Owocik, S.P., Cramer, S.R., & Gayley, K.G., 1996, *ApJ*, 472, L115
- Owocik, S.P., Gayley, K.G., & Cramer, S.R. 1998, in *ASP Conf. Ser. 131, Properties of Hot, Luminous Stars*, ed. by Ian Howarth, (San Francisco:ASP), 237
- Owocik, S.P., & ud-Doula, A., 2003, in *ASP Conf. Ser. 305, Magnetic Fields in O, B, and A Stars*, eds. by L.A. Balona, H.F. Henrichs, & R. M edupe, 350
- Okazaki, A.T., 1997, *A & A*, 318, 548
- Porter, J.M., 1996, *MNRAS*, 280, L31
- Porter, J.M., & Rivinius, T., 2003, *PASP*, 115, 1153
- Sklettebak, A., 1982, *ApJS*, 50, 55
- Sklettebak, A., 1988, *PASP*, 100, 770
- Sklettebak, A., & Snow, T.P., eds. 1987, *IAU Colloq. 92, Physics of Be Stars* (Cambridge: Cambridge Univ. Press)

- Smith, M. A., Henrichs, H. F., & Fabregat, J., eds. 2000, *IAU Colloq. 175, The Be Phenomenon in Early-Type Stars* (ASP Conf. Ser. 214; San Francisco: ASP)
- Struve, O., 1931, *ApJ*, 73, 94
- Telfer, D. C., Brown, J. C., Hanuschik, R., & Cassinelli, J. P., 2003, in *ASP Conf. Ser. 305, Magnetic Fields in O, B, and A Stars*, eds. by L. A. Balona, H. F. Henrichs, & R. M. Edupe, 291
- Telling, J. H., 2000, in *IAU Colloq. 175, The Be Phenomenon in Early-Type Stars*, eds. M. A. Smith, H. F. Henrichs, & J. Fabregat (ASP Conf. Ser. 214; San Francisco: ASP), 422
- Townsend, R., Owocki, S. P., & Howarth, I. D. 2004, *MNRAS*, 350, 189
- ud-Doula, A., & Owocki, S. P., 2002, *ApJ*, 576, 413
- ud-Doula, A., & Owocki, S. P., 2003, in *ASP Conf. Ser. 305, Magnetic Fields in O, B, and A Stars*, eds. by L. A. Balona, H. F. Henrichs, & R. M. Edupe, 343
- Underhill, A., & Doazan, V., eds. 1982, *B Stars with and without Emission Lines* (NASA SP-456, Washington: NASA)
- Yudin, R. V., 2001, *A & A*, 368, 912

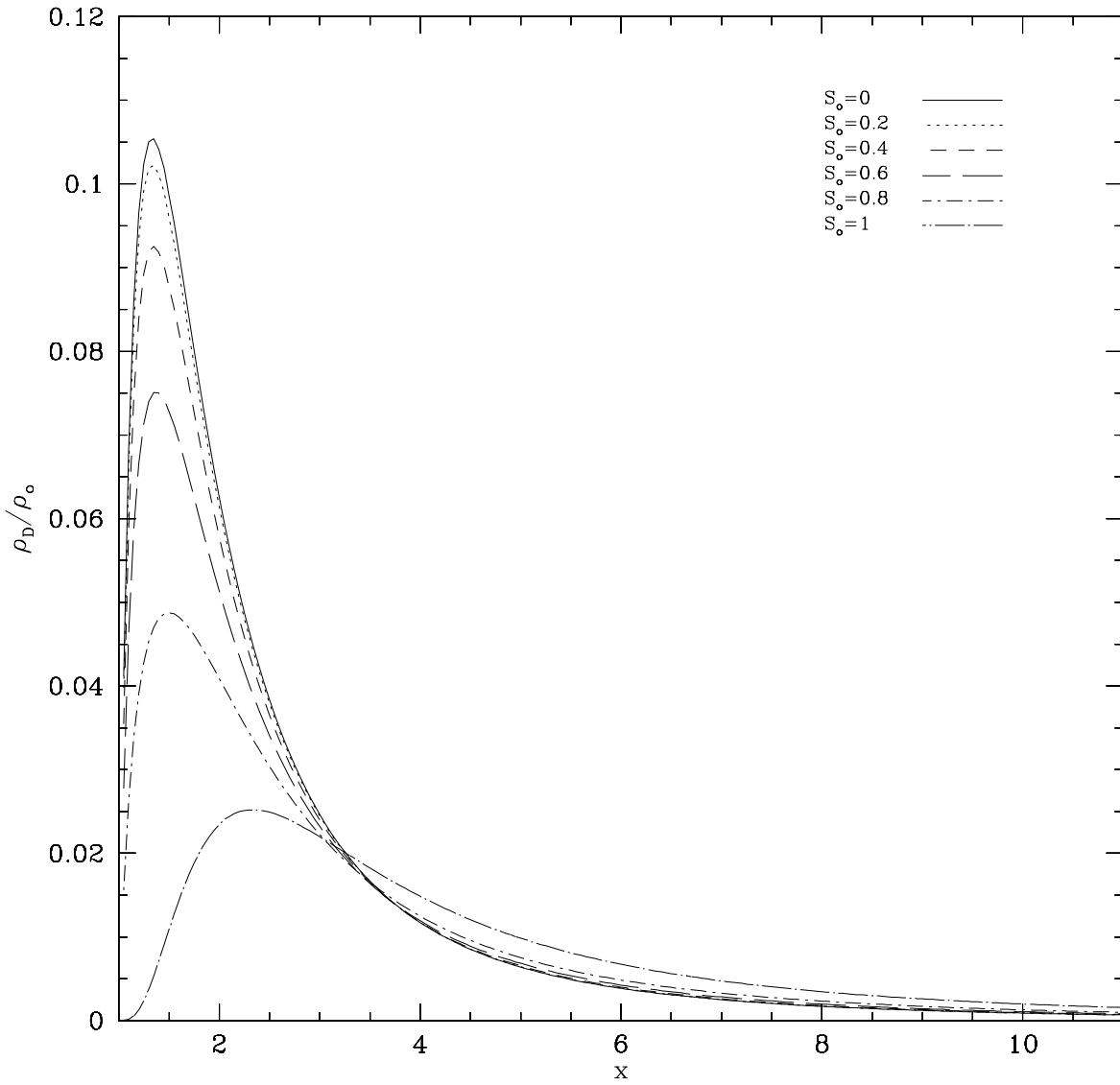


Fig. 1. | Disk density  $\frac{\rho_D}{\rho_0}$  vs equatorial distance  $x$  for various spin rates,  $S_0$ . Disk density increases rapidly then decreases sharply again. The peak value decreases and moves out as  $S_0$  increases, but the peak is in the range  $x = 1.3 - 2.3$  for all  $S_0$ .

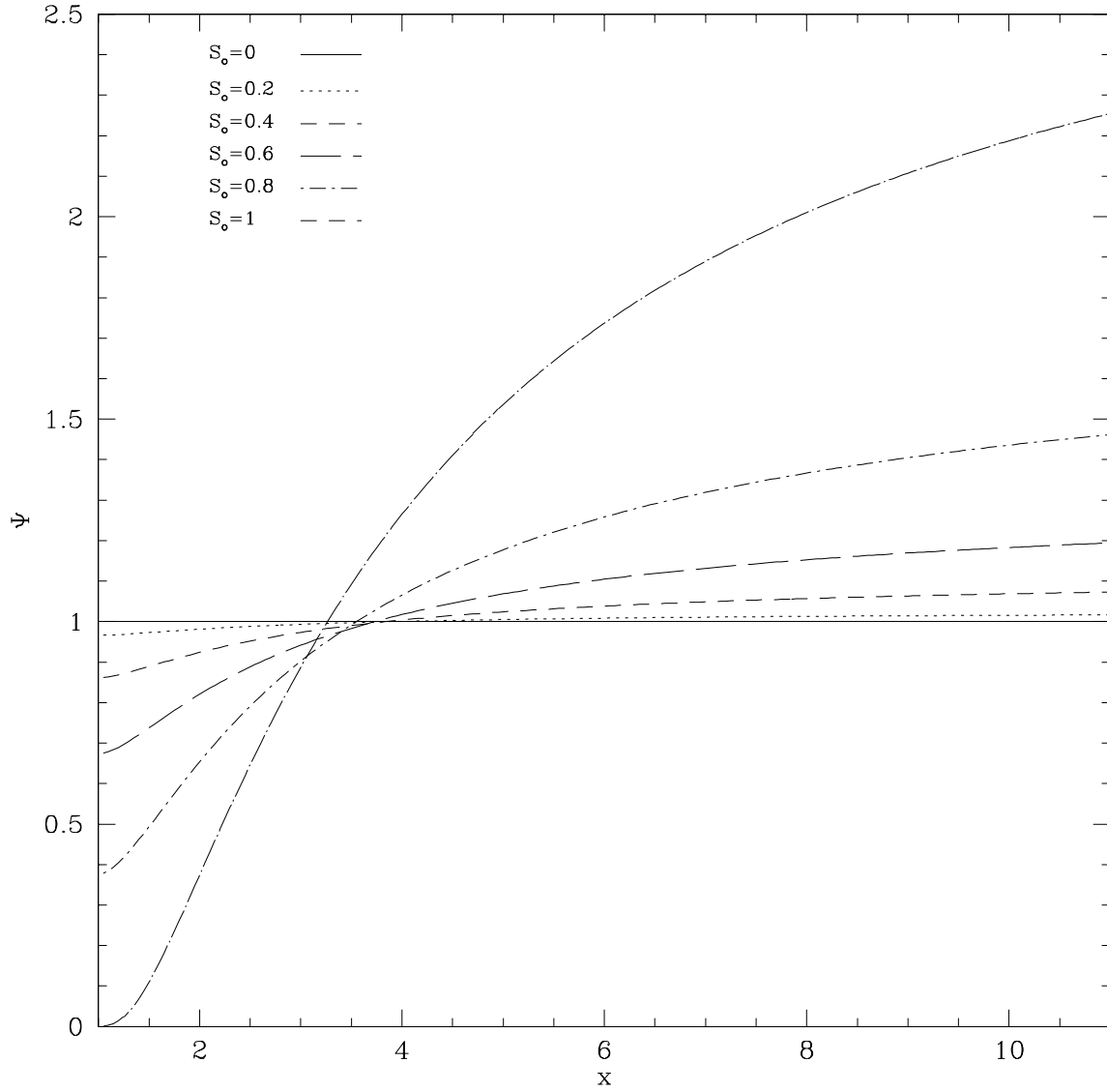


Fig. 2. | Ratio of disk density to that without gravity darkening  $= \frac{\rho_D(S_o, x)}{\rho_D(0, x)}$  vs equatorial distance  $x$  for various spin rates  $S_o$ .

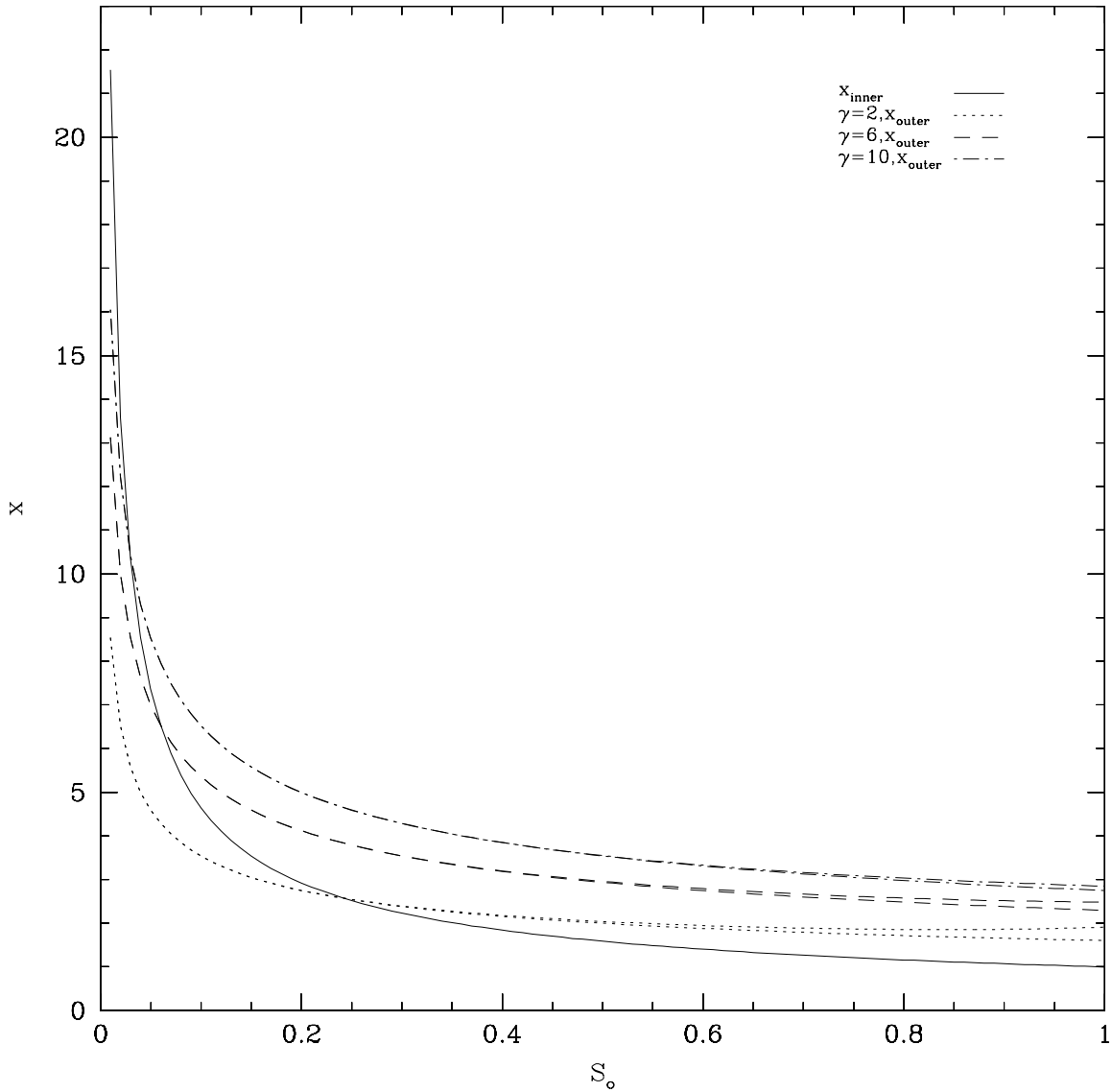


Fig. 3. | Disk boundaries  $x_{inner}$  and  $x_{outer}$  vs  $S_0$  for various  $\gamma$ . The solid line corresponds to the inner radius  $x_{inner}$ , and the other lines to the outer radius of the disk for various  $\gamma$ . Each pair of curves with the same line type gives results with gravity darkening (upper curve) and without gravity darkening (lower curve). For larger  $\gamma$ , one requires smaller  $S_0$  in order for a disk to form ( $x_{outer} > x_{inner}$ ). This implies that for small magnetic fields, a relatively fast spin rate  $S_0$  is necessary, while for large magnetic fields, moderate  $S_0$  is adequate. Comparing curves with and without gravity darkening shows that gravity darkening has only a minor effect on the outer radius of the disk for any given  $\gamma, S_0$ .

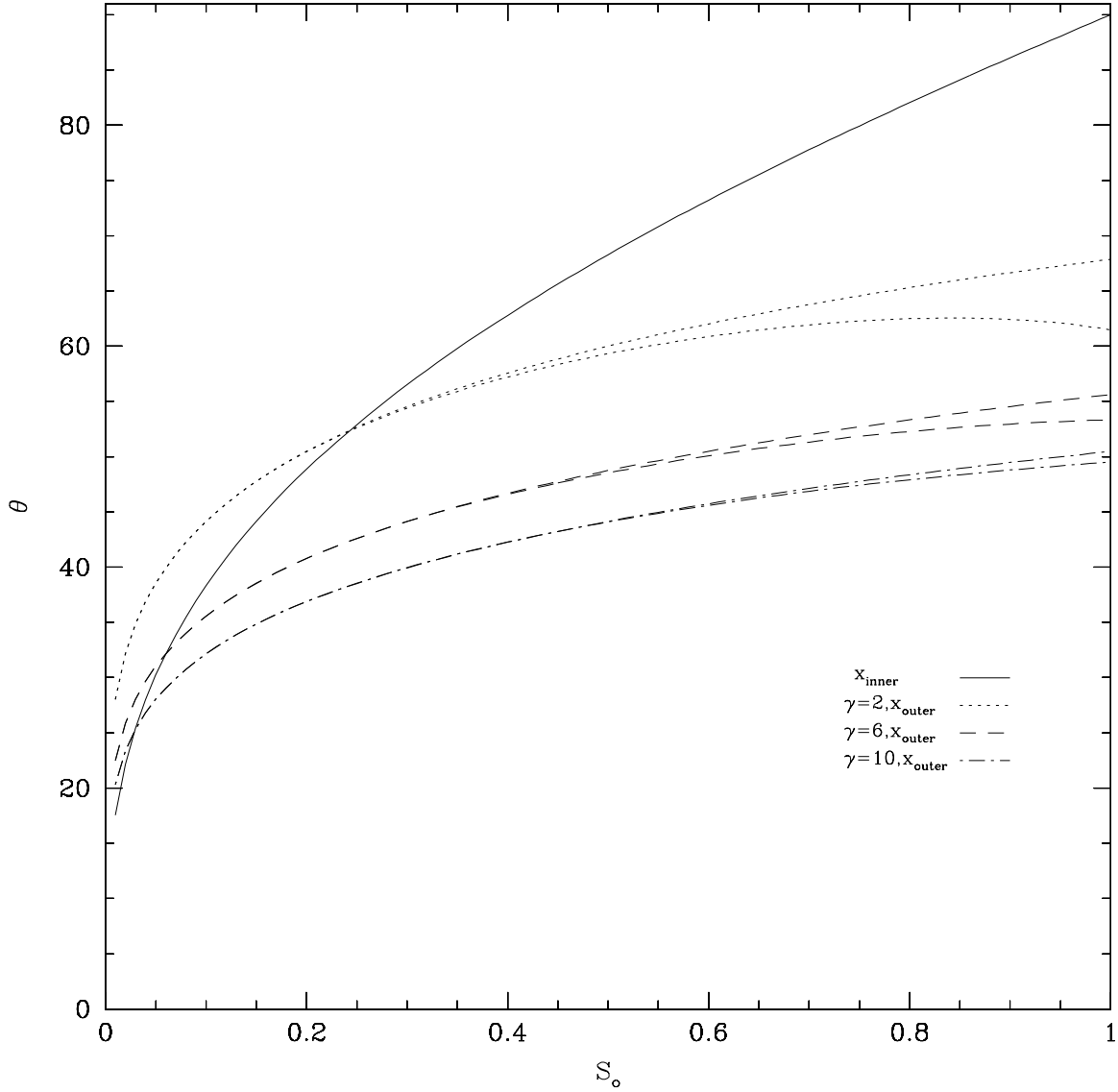


Fig. 4. | Stellar surface colatitudes  $\theta$  corresponding to the inner and outer disk boundaries, vs  $S_0$  for various  $\gamma$ . The solid line corresponds to the inner boundary, and the other lines to outer boundaries of the disk. Each pair of curves with the same line type gives results with gravity darkening (lower curve) and without gravity darkening (upper curve). The possible range of colatitudes channeling matter are angles between the curve of solid line type and the other curve for a given  $\gamma$ .

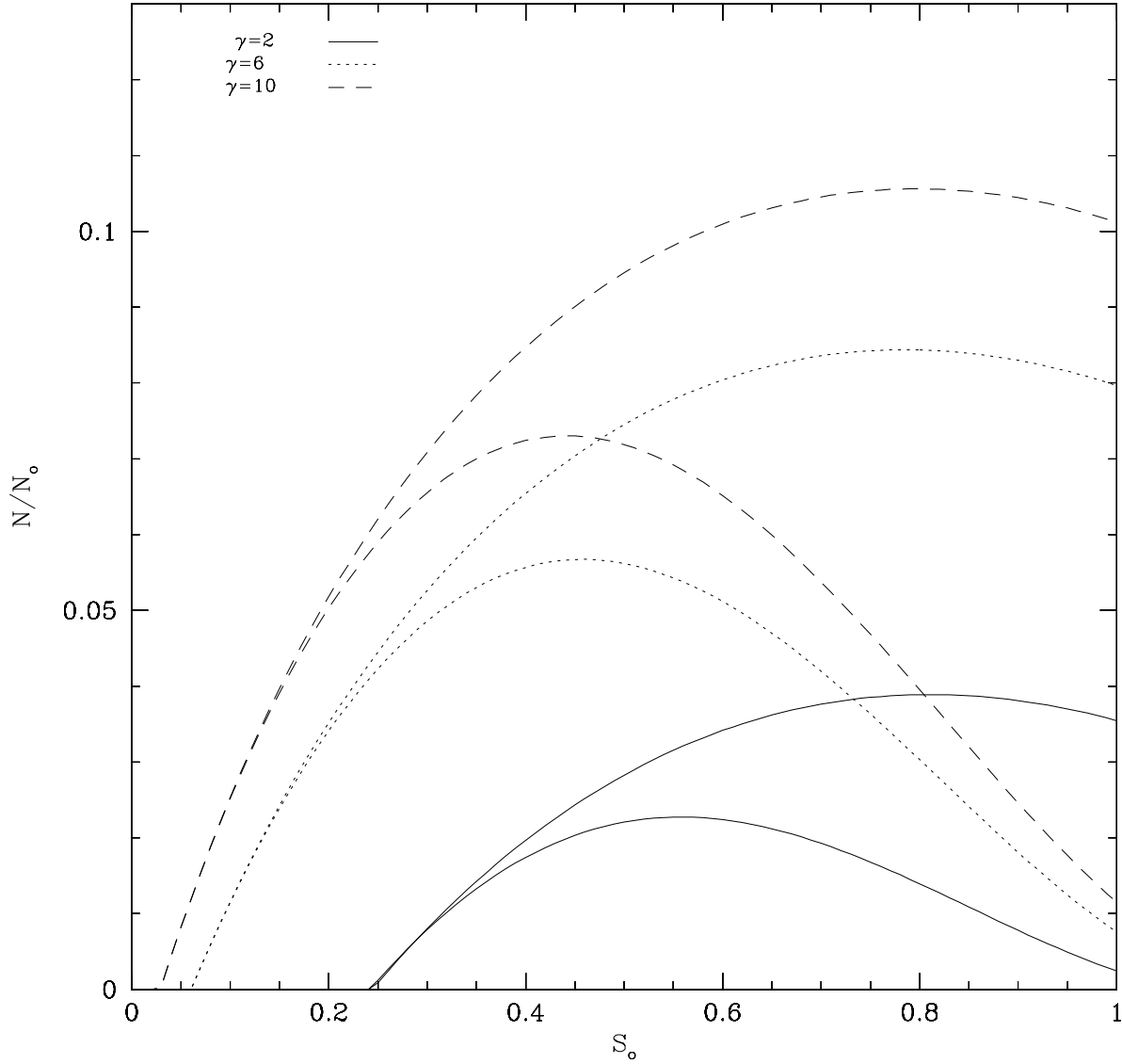


Fig. 5. | Ratio of total number of particles in the disk  $\frac{N}{N_0}$  relative to arbitrary reference value  $N_0$ , vs  $S_0$  for various  $\gamma$ . Lower and upper curves with the same line type are for gravity darkening and no gravity darkening, respectively. Gravity darkening significantly decreases the results as  $S_0$  becomes large, and produces a peak. For larger  $\gamma$ , a smaller  $S_0$  gives rise to the formation of a disk, so the curve becomes wider. The larger  $\gamma$ , the bigger  $\frac{N}{N_0}$ .

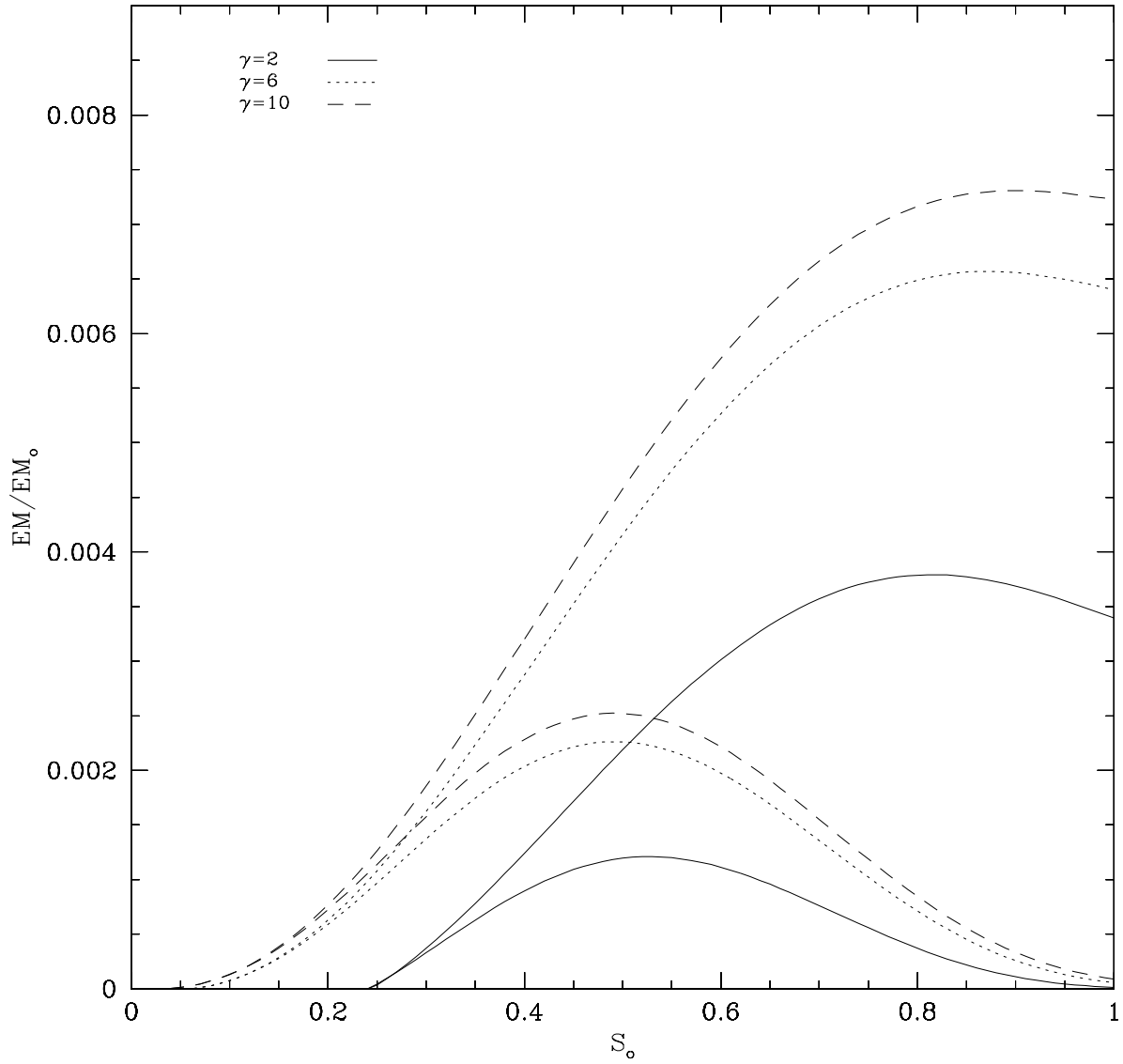


Fig. 6. | Ratio of emission measure  $\frac{EM}{EM_0}$  relative to arbitrary reference value  $EM_0$ , vs  $S_0$  for various  $\gamma$ . Lower and upper curves with the same line type are for gravity darkening and no gravity darkening, respectively.

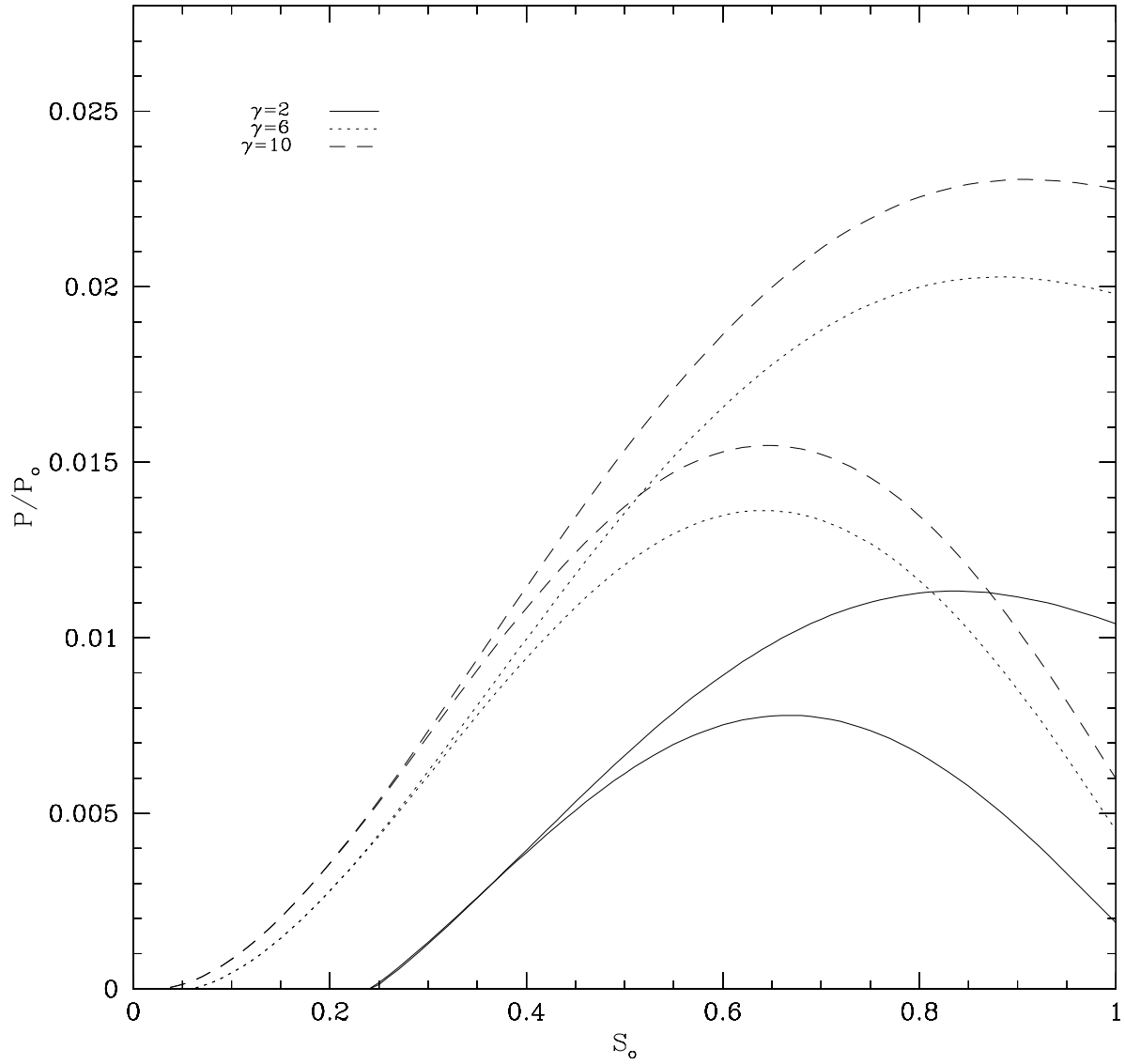


Fig. 7. | Ratio of polarization  $\frac{P}{P_0}$  relative to arbitrary reference value  $P_0$ , vs  $S_0$  for various  $\gamma$ . The inclination angle is assumed to be  $90^\circ$  (edge-on observation). Lower and upper curves with the same line type are for gravity darkening and no gravity darkening, respectively.

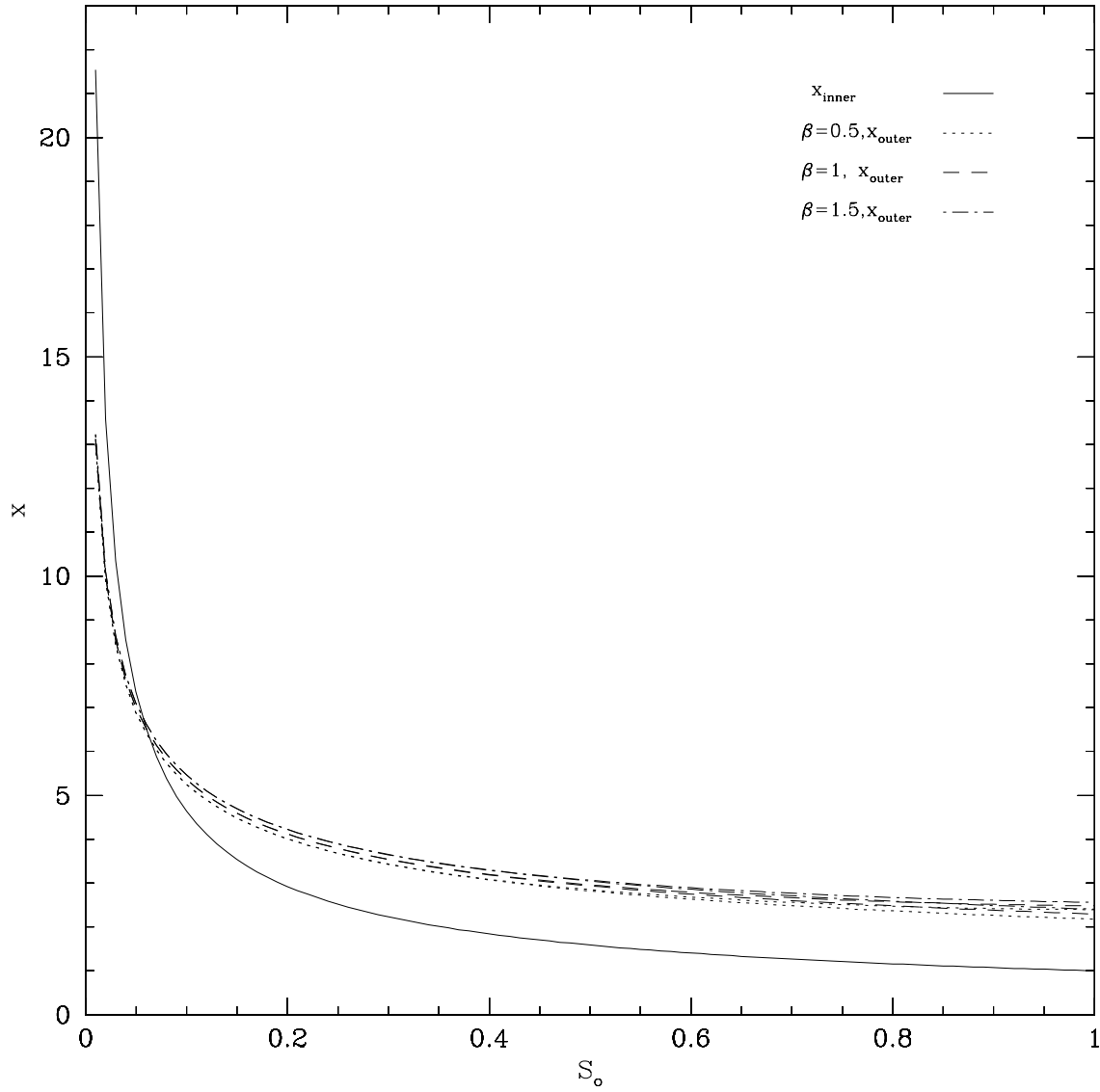


Fig. 8. | Disk boundaries  $x_{inner}$  and  $x_{outer}$  vs  $S_0$  for various  $\beta$  with  $\gamma = 6$ . The solid line corresponds to the inner boundary  $x_{inner}$ , and the other lines to outer boundaries of the disk. Lower and upper curves of the same line type are for gravity darkening and no gravity darkening, respectively.

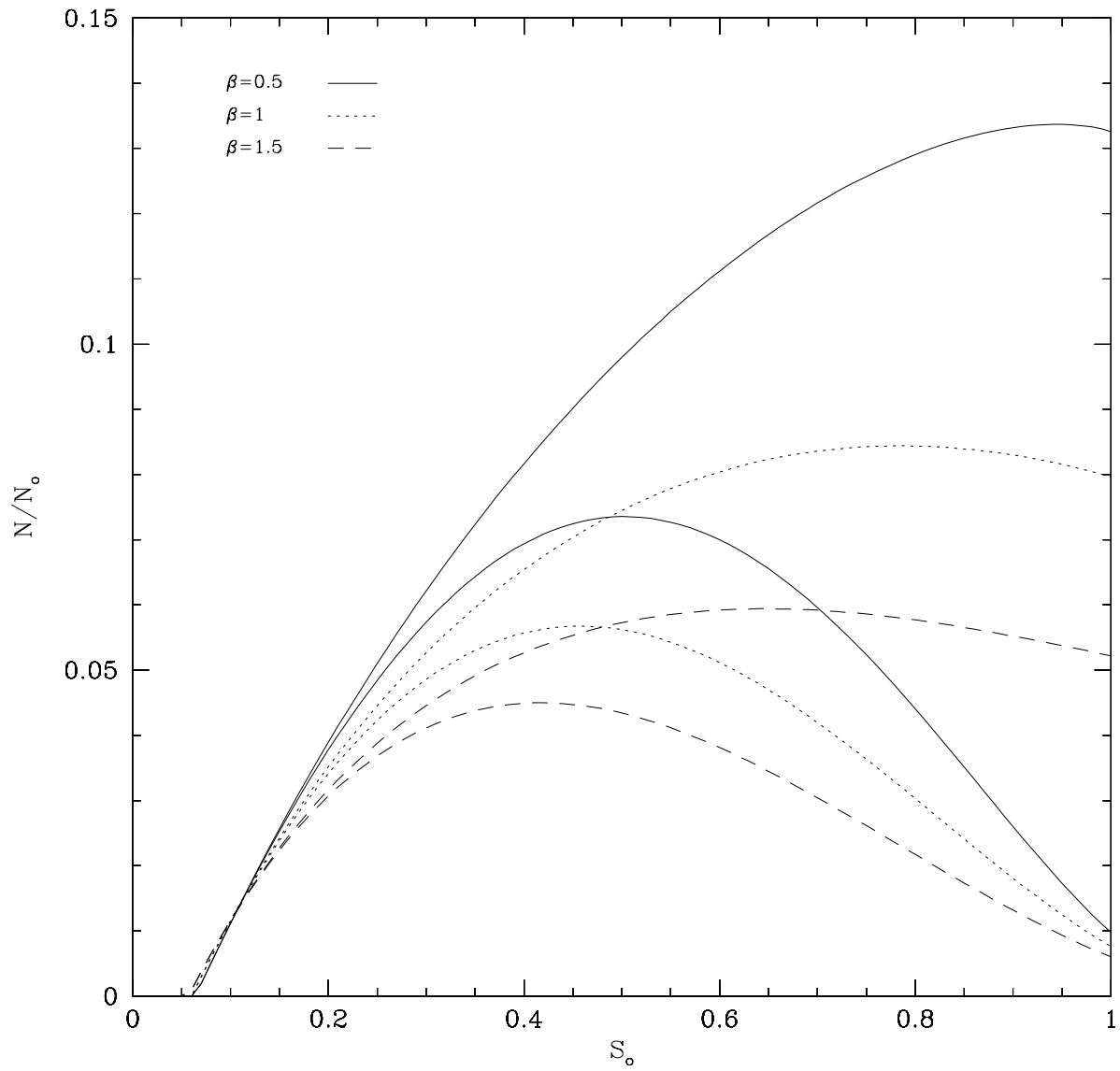


Fig. 9. | Ratio of total number of particles  $\frac{N}{N_0}$  relative to arbitrary reference value  $N_0$ , vs  $S_0$  for various  $\beta$  with  $\gamma = 6$ . Lower and upper curves of the same line type are for gravity darkening and no gravity darkening, respectively.

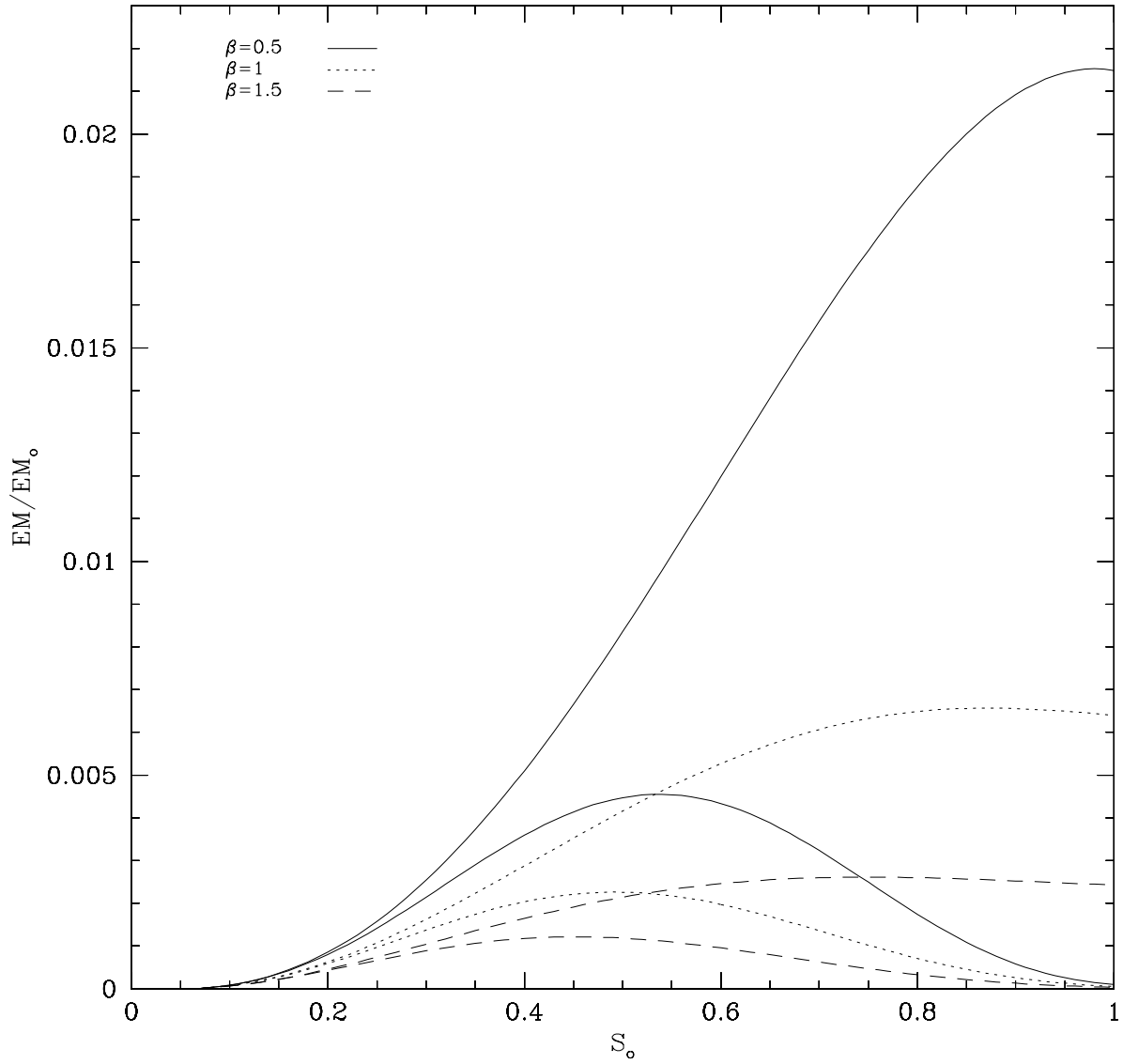


Fig. 10. | Ratio of emission measure  $\frac{EM}{EM_0}$  relative to arbitrary reference value  $EM_0$ , vs  $S_0$  for various  $\beta$  with  $\tau = 6$ . Lower and upper curves of the same line type are for gravity darkening and no gravity darkening, respectively.

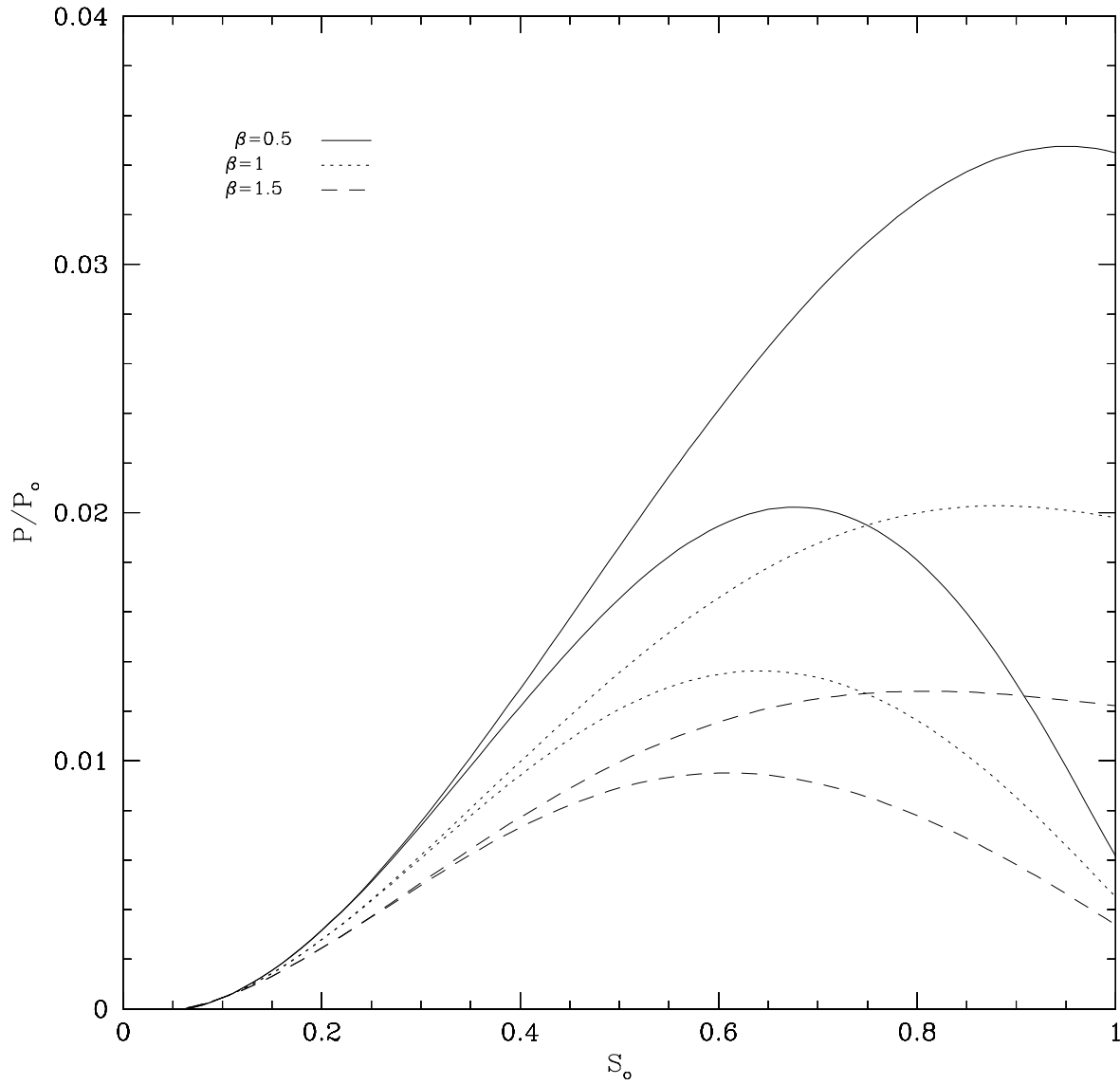


Fig. 11. | Ratio of polarization  $\frac{P}{P_0}$  relative to arbitrary reference value  $P_0$ , vs  $S_0$  for various  $\beta$  with  $\theta = 6$ . The inclination angle is assumed to be  $90^\circ$  (edge-on observation). Lower and upper curves of the same line type are for gravity darkening and no gravity darkening, respectively.